POLITECNICO DI TORINO
Repository ISTITUZIONALE

Experimental validation of laser powder bed fusion simulation

Original
Experimental validation of laser powder bed fusion simulation / Minetola, P., Stiuso, V., Calignano, F., Galati, M., Khandpur, M.S., Fontana, L.. - ELETTRONICO. - (2021), pp. 1-10. (3rd International Conference on Inventive Research in Material Science and Technology (ICIRMCT 2021) Coimbatore (India) 22-23 gennaio 2021) [10.1088/1757-899X/1091/1/012048].

Availability:
This version is available at: 11583/2874532 since: 2021-03-18T01:06:11Z

Publisher:
IOP Publishing

Published
DOI:10.1088/1757-899X/1091/1/012048

Terms of use:

This article is made available under terms and conditions as specified in the corresponding bibliographic description in the repository

Publisher copyright

(Article begins on next page)

15 October 2026

PAPER • **OPEN ACCESS**

Experimental validation of laser powder bed fusion simulation

To cite this article: P Minetola *et al* 2021 *IOP Conf. Ser.: Mater. Sci. Eng.* **1091** 012048

View the article online for updates and enhancements.

The Electrochemical Society
Advancing solid state & electrochemical science & technology
240th ECS Meeting ORLANDO, FL
Orange County Convention Center Oct 10-14, 2021
Abstract submission due: April 9
SUBMIT NOW

Experimental validation of laser powder bed fusion simulation

P Minetola[1], V Stiuso[1], F Calignano[1], M Galati[1], M S Khandpur[1], and L Fontana[1]

[1] Dept. Management and Production Engineering (DIGEP), Politecnico di Torino, Corso Duca degli Abruzzi 24, 10129 - Torino, Italy

paolo.minetola@polito.it

Abstract. In many industrial sectors, laser powder bed fusion (L-PBF) is the main additive manufacturing technology for producing end-usable metal parts. Although L-PBF technique has been developed in the last twenty years, ensuring process feasibility and achieving maximum product quality at the first building session is still a difficult goal to pursue. Simulation software packages are available in the market for the prediction of induced stresses and deformation in L-PBF products to help the user getting the part right at the first time. In this paper, Amphyon software by Additive Works is tested and experimentally validated for the production of Ti6Al4V parts in an EOSINT M270 Dual Mode machine. First, the sensitivity of the software is evaluated by changing the main process parameters by +/- 20% with respect to Ti64 reference values. After calibration, the software is validated by comparison of the predicted deformed shape of a reference part with the real geometry using 3D scanning. Experimental results show that Amphyon software is able to predict the deformed shape for L-PBF parts correctly. The deviations from the real geometry depend on a simplified simulation model that considers a limited set of parameters for the L-PBF process.

1. Introduction

Among Additive Manufacturing (AM) technologies for metals, powder bed fusion (PBF) is the most widespread process for the production of end-usable part directly from a CAD model and without the need for specific tools or dies [1]. In laser powder bed fusion (L-PBF), which is also renowned as Selective Laser Melting (SLM), a laser beam is used to selectively melt metal particles layer after layer until part completion [2].

When compared to subtractive manufacturing, apart from advantages deriving from the higher design freedom, AM makes mass customization viable because of the absence of specific moulds or dies. In AM, the size of the economic lot is pushed down to the single unit of a product and getting a part right at the first time is of paramount importance [3, 4]. This need holds for most AM applications in the biomedical or racing sectors, where a unique part is requested with a specific design and shape that are different from those of other parts [5]. Therefore, especially for parts with a complex shape, optimization of the L-PBF process is fundamental to reduce the defect rate and associated costs, while maximizing part quality and profit.

Unlike the expensive experimental trial and error approach, numerical methods can be used for the optimization of the L-PBF process by means of virtual simulations. Several different approaches have been presented in the literature for the simulation of the L-PBF process [6-18]. The simulation aims to predict the behaviour of the metal powder in the interaction with the laser source during the melting process and the subsequent cooling phase in each layer of the build. The computational methods evaluate the effect of the L-BPF process on the material properties and its impact on the final part geometry and quality [19]. Therefore, virtual simulation is an aid for the optimization of powder bed fusion through

Content from this work may be used under the terms of the Creative Commons Attribution 3.0 licence. Any further distribution of this work must maintain attribution to the author(s) and the title of the work, journal citation and DOI.
Published under licence by IOP Publishing Ltd

the definition of part orientation, support structures, and optimal machine parameters so that residual stresses in the part and the associated geometrical distortions can be minimized [20, 21].

Distortions are the inevitable result of the thermal gradient between the different areas of the powder bed. During the layerwise process, the bed area invested by the spot of the laser beam will have a temperature close to the material melting point. This area is generally named heat-affected zone (HAZ) [22, 23]. Conversely, the temperature of the surrounding areas will be much lower.

The material in the HAZ undergoes thermal expansion and forces the surrounding colder material to bend for accommodating the expansion. When the action of the laser is over, the material in the HAZ cools and its contraction imposes tensile stressing in the underlying layers. The stresses due to the expansion and contraction are so high as to cause permanent plastic deformation. Excessive distortions during the build cause the delamination between the layers with consequent upward bending of the upper part layer. Due to this deformation, the reacoter might collide with the upper layer of the part while depositing the next layer of powder on the bed. Depending on the type of deformation, the collision can lead to the safety stop of the machine with consequent interruption of the construction of the piece or even of the entire job [24]. The remaining parts are incomplete and the corresponding material is a production waste.

To prevent distortions during the L-PBF process, constant heating of the build plate is used to reduce thermal gradients. Moreover, support structures can be added to the part to conduct heat away from the hottest areas of the build. Thus, the addition of supports prevents part distortion and warping as well as cracks induced by thermal stresses. The other main roles of support structures are to fix the part on the build platform and to support overhanging geometries. The number and volume of supports depend primarily on the orientation of the part in the build volume of the AM machine [25, 26]. Since the support structures are made of the same metal as the part, further post-processing and metal cutting operations are needed with an increase of manufacturing times and costs. Hence, the simulation of the L-PBF process allows considering different orientation alternatives, supporting strategies, process parameters and resulting part distortions resulting from the thermal history of the layers in the powder bed.

The general manufacturing route of a metal product by L-PBF involves several different steps and operations (figure 1).

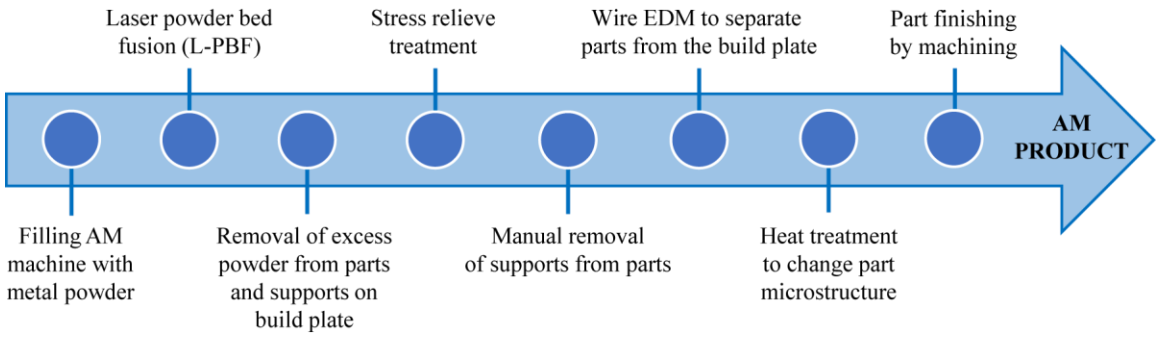

Figure 1. Manufacturing route of a metal part by L-PBF.

First the metal powder is loaded into the feeding the AM machine, then the parts are built layerwise by the L-PBF process. Once the build is complete, the unmelted powder is removed from the build plate to clean the parts that are still fixed by the supports. Before separating the part from the plate, a stress relieve treatment is normally applied to reduce the residual stresses and related part distortions. After this first thermal treatment, supports are manually removed to avoid further part distortions at the separation from the build platform. At this stage, the removal of the support structures reduces the time and cost of the final finishing step. After support removal, the parts are separated from the build plate by wire electro-discharge machining (WEDM) not to cause additional stresses by a mechanical cutting action. Final finishing is needed to remove the material allowance and get parts to their final shape in compliance with dimensional and geometric tolerances. The final machining step might be preceded by

a second thermal treatment for the modification of part microstructure to meet required material properties.

Nowadays most complete simulation methods also consider the effect of stress relieving treatment and the minimization of part warpage by compensation of the geometric distortions [27]. Internal stresses caused by the thermal gradient in the L-PBF process are normally set equal to zero when the simulation includes the stress relieving. Based on the distortion information, software packages for L-PBF simulation compute the compensated shape of the part. If simulation results are reliable, by producing the compensated geometry under the same conditions and inputs of the simulated L-PBF process, the real distorted shape of the AM part should be very similar to the one of the nominal CAD model, i.e. near-net-shaped.

Several software packages for the simulation of the L-PBF process are available in the market [27]. In this paper, Amphyon software is tested for the optimization of powder bed fusion for Ti6Al4V using an EOSINT M270 Dual Mode machine. The experimental equipment and methodology are described in the following section, while experimental results of the calibration and validation of the L-PBF simulations are presented in the third section. Conclusions and future developments are discussed in the last section.

2. Materials and methods

Amphyon software is developed and sold by the German company Additive Works GmbH and is included in the Altair Partner Alliance (APA) program. In this work, the 2020 version of Amphyon, which is the fifth major version since the beta release of 2016, was used. The user-friendly framework consists of five modules to be used in L-PBF chains from the CAD model to the build job, including the stress-relieving treatment and the compensation of geometric distortions.

First of all, the sensitivity of Amphyon software was evaluated by changing the simulation value of the process parameters by +/- 20% with respect to the standard values adopted by the authors for Ti6Al4V powder with an EOSINT M270 Dual Mode machine [28]. The main process parameters are resumed in Table 1 for a layer thickness of 30 µ. The EOSINT M270 has a Ytterbium (Yb) fiber laser source with a power of 200 W for a laser spot of 100 µm. The working volume of the machine is 250 x 250 x 215 mm and the build chamber is filled with argon during the L-PBF process, limiting the oxygen content to 0.1% to reduce the reactivity of the titanium powder.

Table 1. Process parameters of the EOSINT M270 machine for Ti6Al4V.

Parameter	Core	Skin	Contour
Laser power (W)	170	150	120
Laser spot size (µm)	100	100	100
Scan speed (mm/s)	1250	1000	1250
Hatching distance (mm)	0.10	0.10	0.10

Amphyon software uses a unique set of parameters for the simulation of the L-PBF process without distinguishing between the core or skin or contour regions. However, while the skin and contour parameters are set for specific and limited zones of the part in the build layer, the core covers most of the part area in the powder bed if the cross section is not too small. Therefore, the melting of the metal powder and its thermal history are mainly influenced by the laser parameters for the core region. For this reason, the core parameters from Table 1 were used as input for Amphyon simulations together with a build platform temperature of 100 °C. The Ti6Al4V material properties were set as Young modulus of 110 GPa, Yield stress of 1060 MPa and Poisson coefficient of 0.3. These values were extracted from the EOS datasheet for Ti6Al4V powder processes with an EOSINT M270 machine.

A reference geometry provided by Additive Works and named “AW Box” was used for the sensitivity analysis and the subsequent experimental validation. This geometry a hollow thin square tube that is built with the faces oriented at 45 degrees to the build direction and with a vertical edge to support the tube and connect it to the build platform. The tube is designed to be produced without supports. It is 1.67 mm thick and 100 mm long and its overall dimensions are shown in Figure 2.

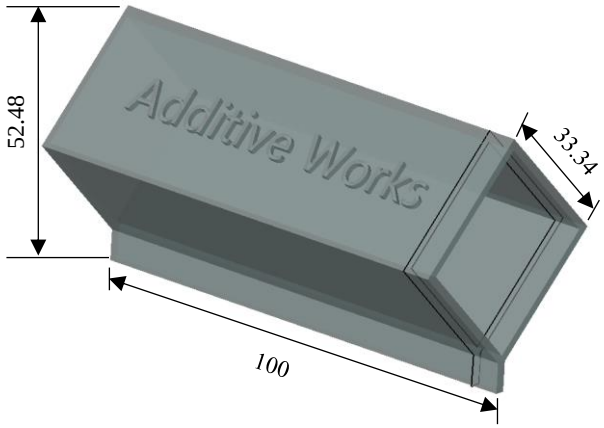

Figure 2. Reference geometry of the hollow square tube with the outline of its cross section.

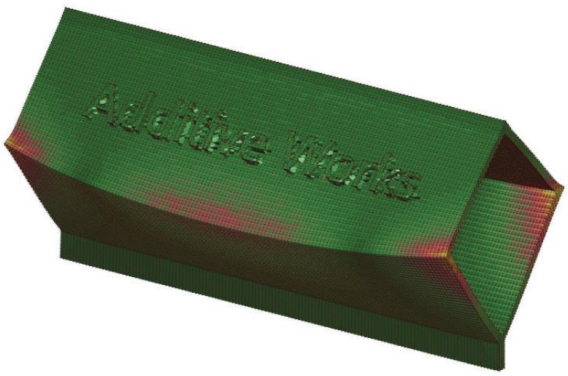

Figure 3. Structure of the mesh for the simulation model in Amphyon software.

Table 2. Settings of the simulation model and solver of Amphyon software.

Parameter	Mechanical simulation	Thermal simulation
Mesh type	Adaptive	Adaptive
Mesh resolution	2	2
Solver accuracy	0.5	0.2

At the end of the sensitivity analysis, the influence of the variation of +/- 20% of the process parameters is considered over the following results of Amphyon simulation: the temperature at the end of the process, maximum residual stress, maximum deformation and build time. In order to avoid differences due to the mesh structure, the properties of the simulation model were not changed in Amphyon software during the analysis. The mesh resolution setting ranges from 0 (coarse) to 10 (fine), whereas the solver accuracy can be set from 0.0 (fast) to 1.0 (accurate). The adopted values for the simulation and solver are listed in Table 2 because the mechanical and thermal simulations are run separately. A mesh resolution equal to 2 and a solver accuracy of 0.5 for the mechanical simulation and 0.2 for the thermal one were selected to limit the computational load and time in a standard notebook. The mesh structure of the simulation model is shown in figure 3.

To account for the specific material and machine, the calibration of the simulation parameters is implemented in Amphyon through an experiment-based approach that requires the use of cantilevers. For precise calibration based on the anisotropy of the material, three samples of the cantilever must be fabricated using a different hatching strategy of the laser beam. The cantilever measures 180 x 7.2 x 8 mm and the three hatching strategies to be considered are the one parallel to the longitudinal direction of the cantilever, the one orthogonal to the first, and the average one, which combines the other two strategies (figure 4). In the specific case of the EOS machine, the main scanning pattern of the laser is rotated by a hatch angle of 67° between consecutive layers.

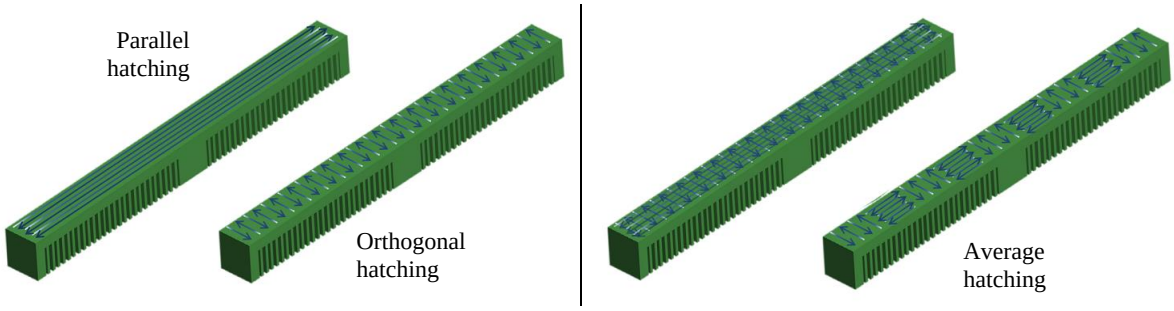

Figure 4. Different hatching strategy of the laser beam to account for material anisotropy.

The three strategies generate a different thermal history in the cantilever with different results in terms of induced residual stresses and consequent bending of the specimen. For the evaluation of the cantilever deformation, it is essential not to apply the stress-relieving treatment to avoid excessive stress relaxation and reduced part distortions. To detach the specimen from the build platform, WEDM cutting should be applied in the longitudinal direction and the maximum deflection of each test specimen along the main axis of the cantilever should be measured.

One replica of the three cantilever specimens and one of the reference geometry (figure 5) were produced with EOS Ti6Al4V powder with 30 µm layer thickness using the EOSINT M270 Dual Mode machine. After manufacturing, dimensional inspection with a structured light 3D Scanner Atos Compact Scan 2M by GOM GbmH was carried out to capture the real geometry of the replicas. The ATOS Compact Scan (figure 6) has two 2 megapixel cameras for stereoscopic vision and a working volume of 125 x 90 x 90 mm. The ATOS scanner uses fringe projection with blue LED light to measure the 3D coordinates of points on the surface of the inspected object through the triangulation principle. According to the acceptance test of VDI/VDE 2634 guideline part 3, the length measurement error of the scanner is smaller than 20 µm. The real geometry of the specimens was acquired before and after separation from the build platform and consequent deformation.

Figure 5. Ti6Al4V replica of the reference square tube by Additive Works.

Figure 6. Inspection of a cantilever using a structured light Atos Compact Scan 2M.

An ECUT32D CNC Wire Cut EDM machine by Suzhou Baoma was used to separate the replicas from the build platform. The cantilever specimens were cut in the longitudinal direction following the indications provided by Additive Works in Amphyon reference guide. The maximum deflection of the specimens was measured using the scan data from the ATOS scanner and the measurement results were used for the calibration of Amphyon software.

After calibration, the production of the reference geometry (figure 2) was simulated using Amphyon. The deformed shape resulting from the simulation was compared to the scan data of the real part for final validation of Amphyon accuracy in predicting L-PBF part distortions.

3. Experimental results

The results of the experimental activities developed following the methodology described in the previous section are described hereafter. The software calibration and all simulations were run on a notebook with Windows 10 Home 64-bit operative system. The PC has an HP 820D motherboard with an Intel(R) Core(TM) i7-6700HQ CPU @ 2.60 GHz, 16 GB RAM, an NVIDIA GeForce GTX960M graphic card and a SATA SSD for data storage.

3.1. Sensitivity analysis

The results of the sensitivity analysis are presented for steps of 10% change of the four simulation parameters (Table 1). These parameters are varied one at a time, so sixteen simulations are run to complete the sensitivity analysis with four levels (-20%, -10%, +10%, +20%) of parameter change. The results of the simulation are displayed in the graphs of figures 7, 8, and 11. The red dashed line in the

graphs shows the reference value that is obtained with the parameters listed in Table 1 for the core region. The temperature at the end of the process (figure 7) increases by almost 10 °C if the laser power is increased by 20%. A reduction of the scan speed or the hatching distance has the effect of delivering more energy per unit area on the powder bed. Therefore, when the scan speed or the hatching distance is reduced by 20%, the temperature at the end of the process is 10 °C higher than with standard parameters. A change of the layer thickness does not influence the temperature at the end of the process.

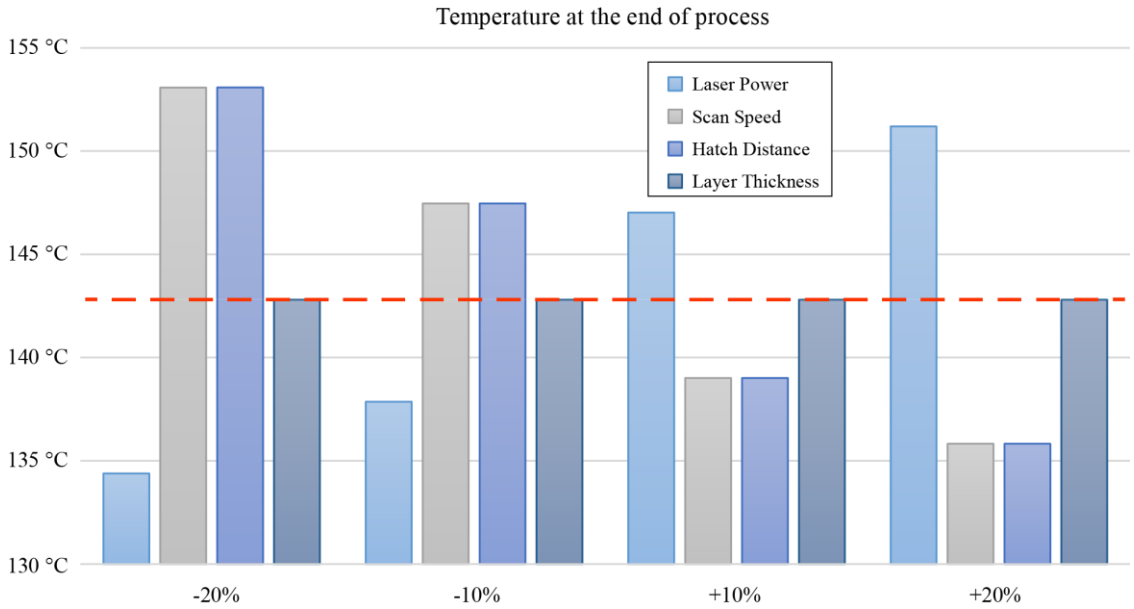

Figure 7. Results of the sensitivity analysis for the temperature at the end of the process.

The influence of the variation of the simulation parameters on the maximum residual stress (figure 8) is similar to one on the temperature at the end of the process. As the laser power increases, the temperature gradient is higher and induced residual stresses grow.

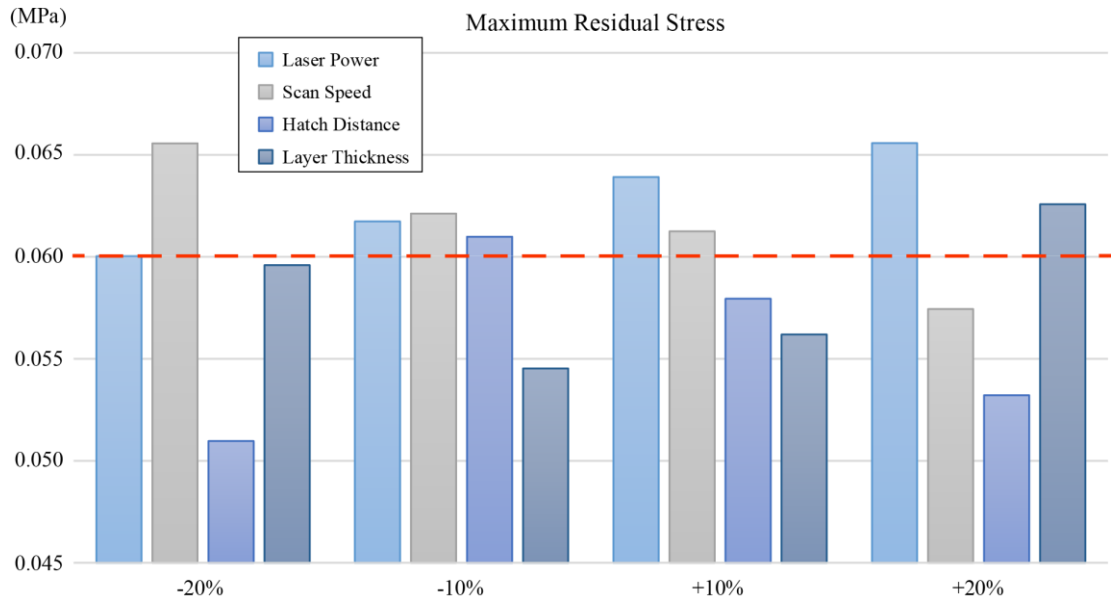

Figure 8. Results of the sensitivity analysis for the maximum residual stress.

The residual stresses for the square cube are concentrated in the red and yellow areas of figure 3, which also shows the structure of the mesh used for the simulation model. The maximum stress is located on the sharp edges that are usually the location where cracks originate due to thermal gradients.

The value of the maximum residual stress ranges from 0.060 MPa for -20% of the laser power to 0.066 MPa when the power of the laser is raised by 20%. Conversely, when the scan speed is increased by 20%, less heat is delivered to the powder bed in the unit time and the maximum residual stress value is 0.057 MPa. By decreasing the scan speed by 20%, the maximum residual stress raises to 0.066 MPa. The variation of the other two parameters of hatching distance and layer thickness from -20% to +20% does not show a clear trend, because the value of the maximum residual stress is oscillating.

To investigate the effect of the simulation parameters on the maximum part deformation, dimensional inspection and comparison of the deformed shape of the square tube are carried out using GOM Inspect software. The deformed shape resulting from the simulation with the standard set of parameters in Table 1 is used as a reference for the comparison. The deformed shape resulting from each simulation of the sensitivity analysis is then aligned to the reference geometry and the comparison results are shown with coloured maps by GOM Inspect (figure 9). The maximum deviation is then measured in the position of the sharp edge where part deformation is maximum, as already shown in figure 3.

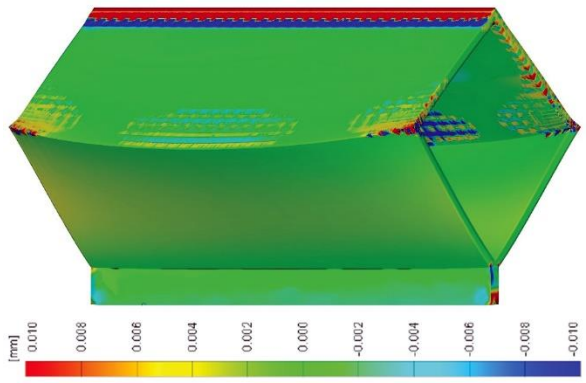

Figure 9. Results of the comparison of maximum deformation for +20% laser power.

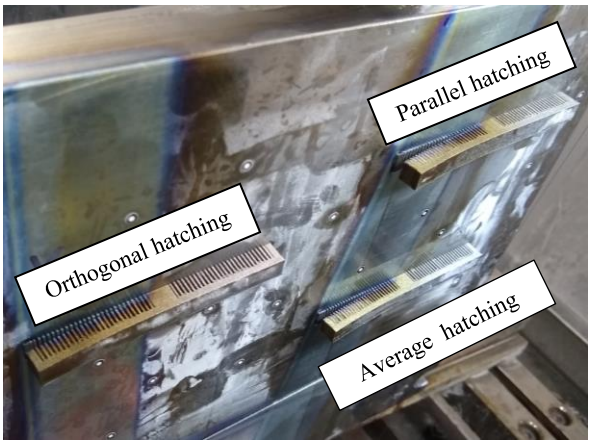

Figure 10. Deformation of the three cantilevers specimens during WEDM.

For the sake of conciseness, the graph with the results of the comparisons about the maximum deformation is omitted. However, since the distortions are a direct consequence of the residual stresses, the trends are similar to those in figure 8. The maximum difference to the deformation with standard parameters is obtained for +20% of the layer thickness. The corresponding maximum distortion is always located on the sharp edge of the square tube and is about 80 µm larger.

Like in all additive manufacturing processes, the build time depends on the part height in the build direction and on the layer thickness, which defines how many layers of material are to be deposited or processed. In the case of the L-PBF process, the hatching distance and scan speed also affect the build time. Accordingly, the results of Amphyon simulations do not show differences in the build time when laser power is varied (figure 11). The increase of the scan speed of the laser provides a small reduction of the build time as the metal powder is melted in less time in every single layer. The same result is obtained when the hatching distance is increased because the exposure to the laser source of the part cross section corresponding to the single layer is completed in a shorter time. The parameter that mainly affects the build time is the layer thickness.

This correct result is in good agreement with the practice. The smaller the layer thickness, the higher the number of layers within the build. When the build volume of the machine is not saturated and a unique small part is produced as in the case of the square tube the recoating operation for depositing the metal powder on the bed takes more time than the exposure and melting of the part cross section. The variation of the scan speed or hatching distance from -20% to +20% shortens the build time from 7 hours

to 6 hours and a half. The modification of the layer thickness from -20% to +20% makes the build time decrease from more than 8 hours to 5 hours and a half. This result is consistent with the real manufacturing time since the build job with the three cantilevers and the reference part was fabricated in about 8 hours.

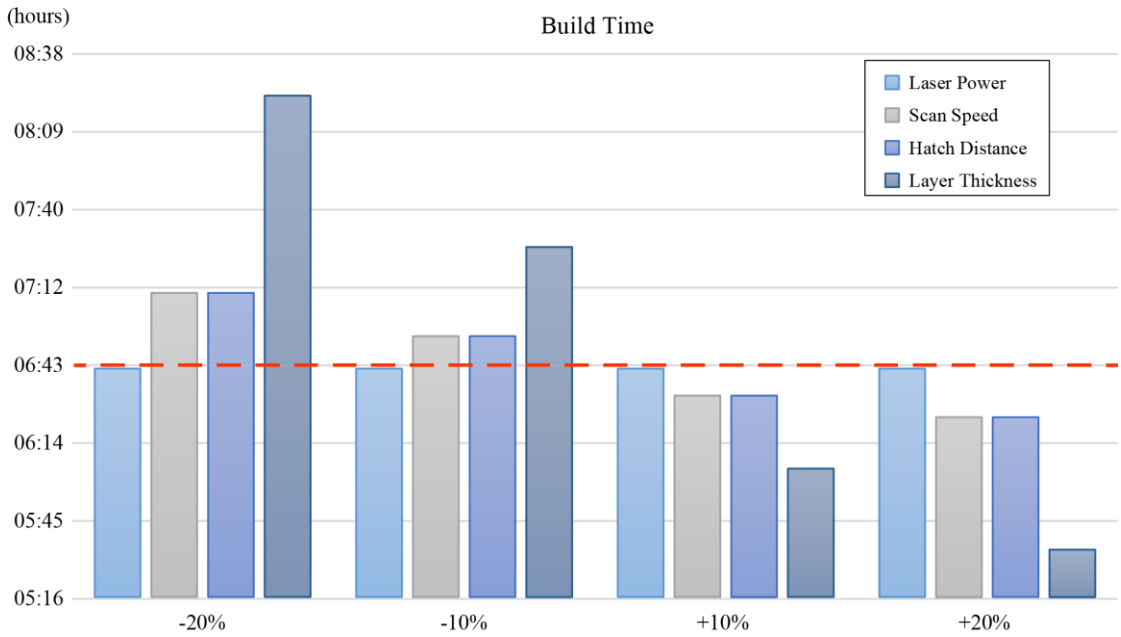

Figure 11. Results of the sensitivity analysis for the build time.

3.2. Calibration of Amphyon software

After the fabrication, the real geometry of the three cantilevers and the one of the square tube are captured using the ATOS Compact Scan before and after the WEDM cut. For the calibration of Amphyon software, the maximum deflection of the three cantilever specimens after separation from the build platform by WEDM is measured. The specimen deformation was visible during the WEDM process as shown in figure 10. The measurements are carried out with GOM Inspect software using the scan data of the ATOS Compact Scan. A reference plane is first defined by best fitting (least-squares method) two sets of points at the two ends of the top surface of each cantilever. The maximum deflection of each specimen is then measured by selecting different points in the middle of the top surface of the cantilever, wherein the distortion is maximum. For each point, the projected distance from the best-fit plane is computed (figure 12). The maximum distances measured for the three cantilevers (Table 3) are used for the calibration of Amphyon software, which takes about 1 hour and a half to be completed.

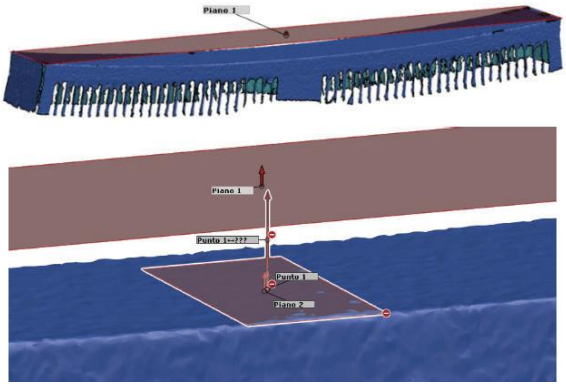

Figure 12. Best fit plane (above) and maximum deflection by the projected point (below).

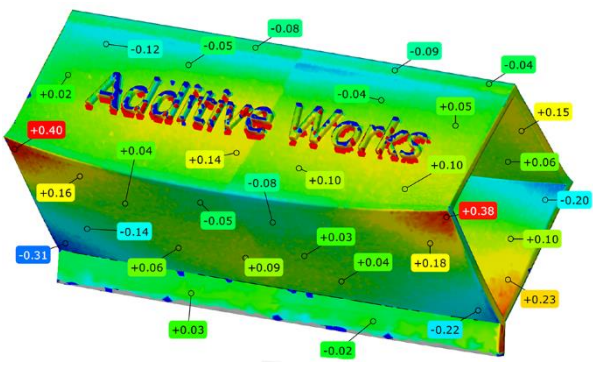

Figure 13. Deviations (in mm) between the real geometry and the deformed shape by Amphyon.

Table 3. Calibration values of Amphyon software from the three cantilever specimens.

Cantilever	Parallel hatching	Orthogonal hatching	Average hatching
Maximum deflection	2.74 mm	2.09 mm	2.28 mm

3.3. Validation

The validation of the simulation results of Amphyon software is carried out by running one last simulation for the square tube after the calibration using the reference process parameters for the core region of Table 1. The deformed shape of the part that was calculated by Amphyon is then exported into the STL format and imported into GOM Inspect software.

In GOM Inspect the simulated geometry is then aligned and compared to the scan data of the square tube after separation from the build platform by WEDM cut. The result of the comparison is shown in figure 13 as a coloured map representing the deviations between the compared shapes. The labels in figure 13 show the local deviations. The statistics provided by GOM Inspect software for the coloured map include an average of 0.05 mm and a standard deviation of 0.30 mm.

The area of the marking of the part with "Additive Works" text is not considered in the following because it is not significant for this study. Generally, the absolute difference between the predicted shape from Amphyon and the real shape of the square tube is below 0.10 mm. In the most stressed areas of the reference part (figure 3), where the deformation is higher, the difference between the compared geometries reaches the maximum of about 0.40 mm. It should also be considered that sharp edges cannot be correctly manufactured by the L-PBF process because the spot of the laser beam has a finite size, that is 0.10 mm in the case of the EOSINT M270 machine.

Therefore, it can be concluded that using the embedded experimental calibration procedure for the material-parameters pair of the specific machine, Amphyon software has good prediction capabilities of the distortion of the as-built part after the L-PBF process.

4. Conclusions

In this paper, the commercial software package Amphyon by Additive Works is tested and validated for the simulation of the L-PBF process using EOS Ti6Al4V powder in an EOSINT M270 Dual Mode machine. As a case study for the analysis, the reference geometry of the "AW Box" by Additive Works was used.

First, a sensitivity analysis is carried out to investigate how a small variation of the main process parameters is taken into consideration by Amphyon solver and related simulation results. Then the software for experimentally calibrated through the production of three cantilever specimens to account for the anisotropy of the material.

After calibration, the production of the reference part was simulated with Amphyon and the resulting deformed shape was compared with the real geometry of the as-built part, which was digitized by 3D scanning. The comparison shows that Amphyon software can correctly predict the distortion induced by the thermal history of the material during the L-PBF process. For the case study, the average difference between the predicted shape from the simulation and the real shape was 0.05 mm, while the maximum deviation was smaller than 0.50 mm.

However, one important feature of Amplyon software was not tested in this work. With its pre-deformation (PRE) module, the software can compensate for the residual distortions of the L-PBF process and can compute a pre-compensated geometry. This geometry can be exported as an STL file and used as the input in the Additive Manufacturing route to get the as-build part with the desired geometry equal to the one of the nominal CAD model. The analysis of the PRE module is ongoing at the Centre of Integrated Additive Manufacturing (IAM@PoliTO) of the Politecnico di Torino and the authors will present the results of their study in a future paper.

Acknowledgments

The authors gratefully acknowledge Mr. Nils Keller, CEO of Additive Works GmbH, for granting a free educational license of Amphyon software to be tested at the Centre of Integrated Additive Manufacturing (IAM@PoliTO) of the Politecnico di Torino.

References

[1] Atzeni E and Salmi A 2012 *Int. J. Adv. Manuf. Tech.* **62**(9-12) 1147-55
[2] Calignano F *et al.* 2017 *Proc. IEEE*, **105**(4) 593-612
[3] Atzeni E, Iuliano L, Marchiandi G, Minetola P, Salmi A, Bassoli E, Denti L and Gatto A 2013 Additive manufacturing as a cost-effective way to produce metal parts *High Value Manufacturing* ed PJ Bartolo et al. (London: CRC Press) pp 3-8
[4] Salmi A, Calignano F, Galati M and Atzeni E 2018 *Virtual Phys. Prototyp***. 13**(3) 191-202
[5] Calignano F, Galati M, Iuliano L and Minetola P 2019 *J. Healthc. Eng*. **2019** 9748212
[6] Papadakis L, Loizou A, Risse J and Schrage J 2014 *Proc. CIRP* **18** 90-5
[7] King W, Anderson AT, Ferencz RM, Hodge NE, Kamath C and Khairallah SA 2015 *Mater. Sci. Tech.* **31**(8) 957-68
[8] King WE, Anderson AT, Ferencz RM, Hodge NE, Kamath C, Khairallah SA and Rubenchik AM 2015 Applied Physics Reviews **2**(4) 041304
[9] Li C, Fu CH, Guo YB and Fang FZ 2016 *J. Mater. Process. Tech.* **229** 703-12
[10] Dunbar AJ, Denlinger ER, Gouge MF and Michaleris P 2016 *Addit. Manuf.* **12** 108-20
[11] Bugatti M and Semeraro Q 2018 *Addit. Manuf.* **23** 329-46
[12] Koepf JA, Gotterbarm MR, Markl M and Körner C 2018 *Acta Mater.* **152** 119-26
[13] Moges T, Ameta G and Witherell P 2019 *J. Manuf. Sci. E.-T. ASME* **141**(4) 040801
[14] Mayer T, Brändle G, Schönenberger A and Eberlein R 2020 *Heliyon* **6**(5) e03987
[15] Olleak A and Xi Z 2020 *Manuf. Lett.* **24** 140-4
[16] Cook PS and Murphy AB 2020 *Addit. Manuf.* **31** 100909
[17] Ninpetch P, Kowitwarangkul P, Mahathanabodee S, Chalermkarnnon P and Ratanadecho P 2020 *AIP Conf. Proc.* **2279**(1) 050002
[18] Hodge NE 2020 *Addit. Manuf.* **37** 101600
[19] Borovkov AI, Maslov LB, Ivanov KS, Kovaleva EN, Tarasenko FD and Zhmaylo MA 2020 *IOP Conf. Ser.: Mater. Sci. Eng.* **986** 012033
[20] Salmi A, Piscopo G, Atzeni E, Minetola P and Iuliano L 2018 *Proc. CIRP* **67** 191-6
[21] Ramesh Sagar V, Lorin S, Wärmefjord K and Söderberg R 2020 *J. Manuf. Sci. E.-T. ASME* **2020** 1-35
[22] Luo Z and Zhao Y 2018 *Addit. Manuf.* **21** 318-32
[23] Roy M and Wodo O 2020 *Addit. Manuf.* **32** 101017
[24] Kayacan MY, Özsoy K, Duman B, Yilmaz N and Kayacan MC 2019 *Mater. Manuf. Process.* **34**(13) 1467-75
[25] Jiang J, Xu X and Stringer J 2018 *J. Manuf. Mater. Process.* **2**(4) 64
[26] Bartsch K, Lange F, Gralow M and Emmelmann C 2019 *J. Laser Appl.* **31** 022302
[27] Peter N, Pitts Z, Thompson S and Saharan A 2020 *Addit. Manuf.* **36** 101531
[28] Minetola P, Galati M, Calignano F, Iuliano L, Rizza G and Fontana L 2020 *Proc. CIRP* **88** 399-404